Helical Graphene Nanostructures Embedded with an Azulene Cluster

Naoki Ogawa, Yousuke Yamaoka, Hiroshi Takikawa, Ken-ichi Yamada,[#] and Kiyosei Takasu[*]

[1]Graduate School of Pharmaceutical Sciences, Kyoto University, Yoshida, Sakyo-ku, Kyoto 606-8501, Japan

[#]Current address: Graduate School of Pharmaceutical Sciences, Tokushima University, Shomachi, Tokushima 770-8505, Japan

[*]e-mail: kay-t@pharm.kyoto-u.ac.jp

Abstract

An azulene cluster is a structural defect of graphenes, and it alters the electronic, magnetic, and structural properties of graphenes and graphene nanoribbons. However, detailed experimental investigations of graphenes or graphene nanostructures embedded with an azulene cluster are limited because they are difficult to synthesise. Herein, azulene-embedded graphene nanostructures (AGNs) were synthesised by following a newly developed synthetic protocol. The nanostructures comprising pentagons, hexagons, and heptagons has three characteristic edges, viz., zigzag-, armchair-, and cove-type edges. Experimental and theoretical investigations of the properties of AGN revealed that

the cove edge has stable helical chirality with a racemisation barrier of 29.2 kcal/mol, in contrast to

normal cove-type edges that undergo rapid racemisation. The in-solution self-association behaviour

and the structural, electronic, and electrochemical properties of AGN are also described in detail.

Graphical Abstract
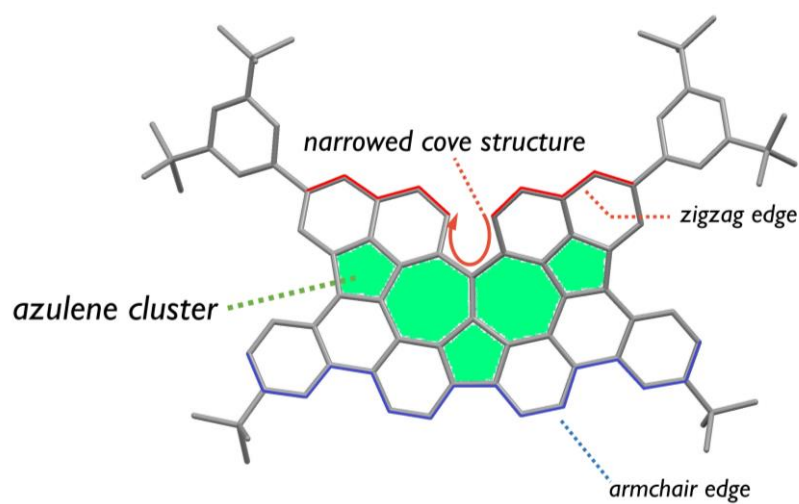
The topology of π-electrons is one of the most crucial factors that determine the properties of graphene nanostructures. Accordingly, much effort has been devoted towards synthesising and elucidating the properties of topologically diverse graphene nanostructures, whose hexagonal rings are fused in different patterns.[1–4] Researchers have also been interested in introducing non-hexagonal rings such as pentagons,[5–7] heptagons,[8–10] or octagons[11] into π-conjugation systems to achieve unique optical, electronic, and structural properties, distinct from those of π-systems composed of only hexagonal units.

Among the non-hexagonal ring systems, the contiguous pentagon–heptagon ring system, the so-called azulene structure, has been attracting considerable interest owing to its interesting properties such as a low-lying excited state and high dipolar moment, which are distinct from those of usual benzenoids.[12] Thus, considerable efforts have been dedicated to incorporate azulene structures into polycyclic aromatic hydrocarbons (PAHs) to impart unique structural and electronic properties.[13–17] Of particular interest is the azulene structure observed in graphenes as one of the structural defects, which breaks the symmetry of graphenes to significantly alter their mechanical, magnetic, and electronic properties, as well as open non-zero band gap.[18–21] It is noteworthy that the azulene units in a single graphene molecule not only exist separately, rather tend to accumulate to form clusters.[21] In graphene nanoribbons (GNRs), whose edge structures are important for their properties, the incorporation of azulene units results in unique edge structures. For example, the GNR bearing

sandwiched contiguous azulene rings would have a zigzag edge and an armchair at the top and the

bottom sides, respectively (Fig 1a). A "narrowed" variant of the cove-type edge[22–26] (Fig. 1c) can

also be considered as another example, where the "cove" comprises a contiguous 6–7–7–6 ring

system instead of the four hexagons of a normal cove edge (Fig. 1b), leading to a narrower cove
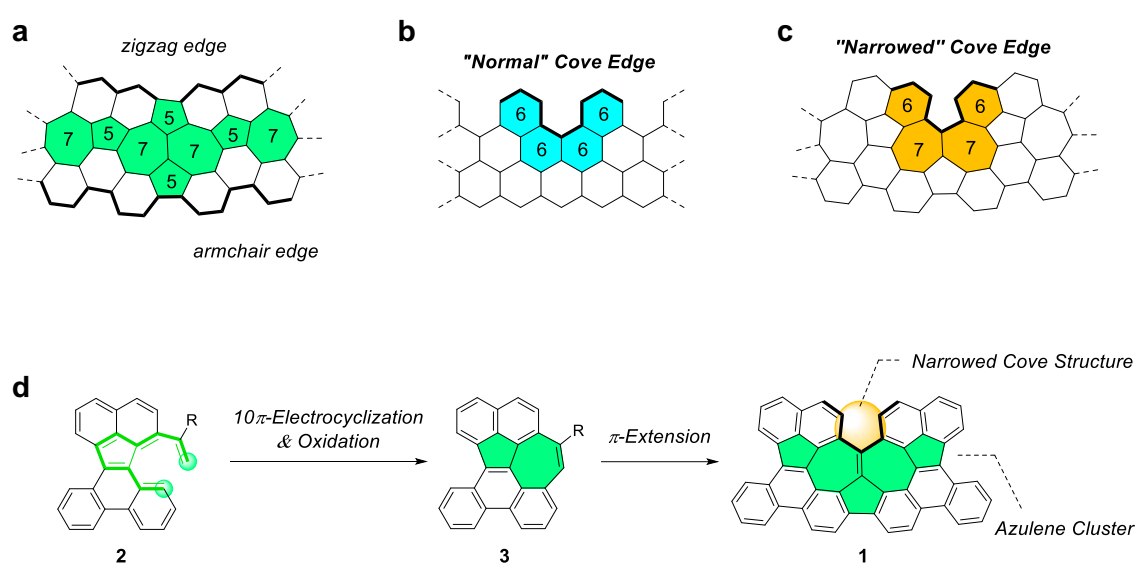
structure.

Fig. 1: Azulene-emmbedded graphenes and graphene nanostructures. **a**, One example of a

graphene nanoribbon containing clusters of azulene units. **b**, Structures of "normal" cove edge. **c**,

"Narrowed" variant of cove edge. **d**, Structural design and synthetic strategy of nanographene **1**.

While there were considerable efforts to theoretically elucidate the nature of azulene-embedded

graphenes and GNRs,[18–21] detailed experimental investigations are still limited, probably due to their

poor availability. Although several approaches based on chemical vapour deposition (CVD)

techniques are emerging, a precise synthesis of the structurally uniform graphenes with azulene units is not straightforward since isomerisation among 5-, 6-, and 7-membered rings occurs on metal surfaces at elevated temperatures under typical conditions of the CVD process.[27,28] Bottom-up chemical synthesis of nanocarbons that resemble model structures of such graphenes would be one solution to this problem.[29–31] Since direct investigation of graphenes embedded with azulene units is challenging due to the difficulty in synthesis, it is of significance to prepare model nanocarbons to gain insights into the properties of parent graphenes. Compared to those of other nanocarbons composed only of hexagonal rings and isolated non-hexagonal ring(s),[29–31] the bottom-up chemical syntheses of nanocarbons with multiple azulene units are still limited, because of the absence of reliable methods, especially in-solution ones.[32–34] Peña, Pascual and co-workers,[35] and Müllen, Fasel, Feng and co-workers[36] elegantly addressed this situation by utilising on-surface dehydrocyclisation of rationally designed precursors to incorporate azulene units into nanocarbons. Mastalerz[37] and Zhang[38] also independently achieved in-solution synthesis of highly fused azulene units via the Scholl cyclisation of ingeniously tailored precursors. Despite these pioneering works, there is still a lack of appropriate methods to construct highly condensed azulene clusters, structures that frequently appear in graphenes.[21] Therefore, new synthetic protocols should be developed to access nanocarbons embedded with this moiety.

Herein, we report a bottom-up chemical synthesis of azulene-embedded graphene nanostructures

1 and their properties (Fig. 1d). Compounds **1** have unprecedented contiguous azulene structures condensed at their heptagonal rings, and it was designed as a model structure of one of the clustering azulene units observed in graphenes. It also has a helical structure considered to be a minimum structure of one of the narrowed variants of the cove-type edge. A newly developed 10π-electrolysation–oxidation cascade of fluoranthene **2** to construct an azulene structure enabled us to obtain the key intermediate **3**, leading to the successful generation of a highly condensed azulene cluster via further π-extension.

Results and discussion

In our continuing studies on PAHs,[39] we reasoned that constructing an additional heptagonal ring next to the pentagon of benzo-fused fluoranthene **2** would be a straightforward way to obtain condensed azulene structure **3**, because **2** itself has a pentagonal ring surrounded by multiple benzene rings (Fig.1d). Unfortunately, it was found that conventional π-extension reactions such as metal-catalysed cycloisomerisation of alkyne, intramolecular Friedel–Crafts acylation, and Scholl cyclisation are not applicable for this purpose, as these reactions led to the formation of complex mixtures or recovery of unreacted starting materials (see Supporting Information for details). After several investigations, it was established that compound **2c** consisting of an α-styryl moiety is a suitable precursor to generate the desired azulene unit. Thus, activating this molecule by visible-

light-irradiation in the presence of an oxidant resulted in a clean conversion of **2c** into **3c** via an

oxidative cyclisation process (Fig. 2a, Eq. 1). The utilisation of visible light as a mild energy source

was important to effectively generate the azulene structure since the activation of **2c** by both UV

light (low-pressure mercury-vapour lamp), which is conventionally used to promote 6π-

electrocyclisation of stilbenes,[40] and heating to 250 °C led to lower yields of **3c** (52 or 40% yield,

respectively). Since **2c** has a 10π-electron system, this oxidative cyclisation reaction would proceed

via a visible-light-promoted 10π-electrocyclisation[41,42] followed by a dehydrogenation by the

oxidant. Such an approach for azulene rings based on oxidative electrocyclic ring closure of the

heptagon is an unprecedented one, to the best of our knowledge. The synthetic utility of this newly

developed method was highlighted by applying it in the synthesis of boronate ester **3a** from **2a** (Fig.

2a, Eq. 2), as the C–B bond on its heptagon was converted into C_{sp2}–C_{sp2} bonds by a transition-metal

catalysed cross-coupling reaction such as the Suzuki coupling reaction, offering opportunities for
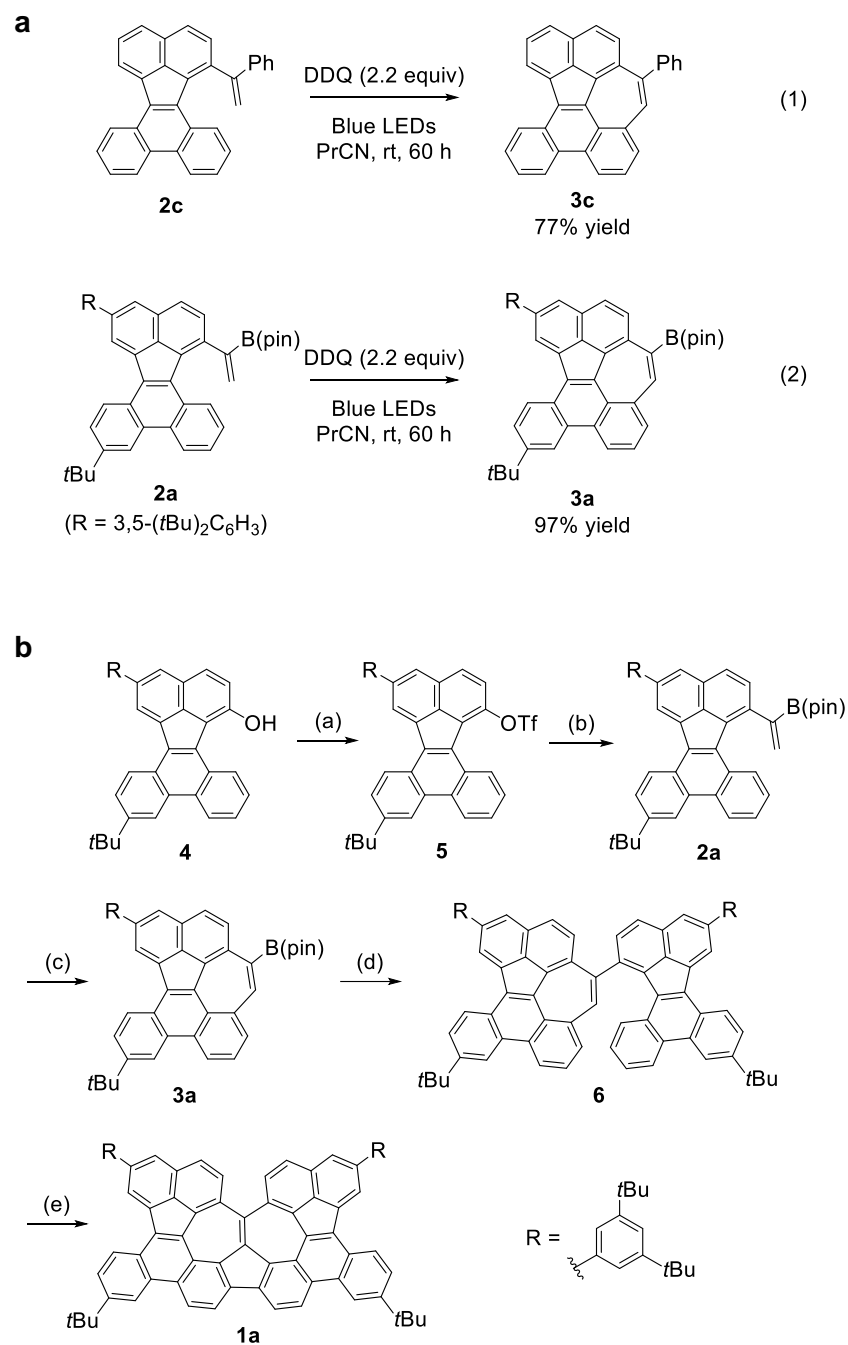
further π-extensions.[43]

Fig. 2: Synthetic protocol for the azulene units. a, Conversion of dibenzofluoranthene **2** into

azulene 3 via visible-light-promoted oxidative cyclisation. **b**, Synthesis of AGN **1a.** Reaction

conditions: (a) Tf$_2$O, DIPEA, DCM, 25 °C (b) CH$_2$=C(Bpin)$_2$, K$_3$PO$_4$, Pd(PPh$_3$)$_4$, dioxane, 100 °C,

69% yield; (c) DDQ, butyronitrile, blue LEDs, 25 °C, 97% yield; (d) **5**, K$_3$PO$_4$, Pd(PPh$_3$)$_4$, dioxane,

100 °C, 46% yield; (e) DDQ, TfOH, DCM, 25 °C, 5 min, 16% yield. Tf = trifluoromethanesulfonyl;

DIPEA = diisopropylethylamine; DCM = dichloromethane; pin = pinacolate; DDQ = 2,3-dichloro-

5,6-dicyano-p-benzoquinone; LED = light emitting diode.

With azulene-embedded boronate ester **3a** in hand, we moved forward to the synthesis of

graphene nanostructure **1** (Fig. 2b). The cross-coupling reaction between boronate ester **3a** and

triflate **5**, which was prepared by the triflylation of hydroxyfluoranthene **4**,[39] proceeded smoothly to

generate compound **6** in 46% yield. The Scholl reaction of compound **6** using the combination of

2,3-dichloro-5,6-dicyano-p-benzoquinone (DDQ) and trifluoromethanesulfonic acid (TfOH) resulted

in the formation of two C–C bonds to afford the desired graphene nanostructure **1a** in 16% yield.

The purple crystals of compound **1a** suitable for X-ray crystallography were obtained by

recrystallising it from a NO_2Ph/CS_2/cyclohexane solvent system by slow solvent evaporation, and its

structure was unambiguously confirmed (Fig. 3a).[44] The bond lengths of the pentagonal and

heptagonal rings in compound **1a** are summarised in Fig. 3b together with those of the unsubstituted

azulene.[45] The azulene structures in compound **1a** show significant bond alternation varying between

1.33 Å and 1.50 Å, as observed in the unsubstituted azulene. The armchair-edge-like side of **1a**,

shown as the bottom side in the figure, has a rather planar structure, and **1a** was stacked together on

that side in the crystal form (Fig. 3c and 3d). The cove region of compound **1a** has, in contrast, a

significantly distorted helical structure, and the angle of the eclipsed rings (shown as B and B' in Fig. 5a) is 39°, the value is close to that reported for the normal cove edge (38°).[22] The enantiomers arising from this cove region were alternatively arranged in the crystal structure with a distance as short as 3.2 Å, suggesting strong intermolecular π−π stacking interactions (Fig. 3c and 3d).
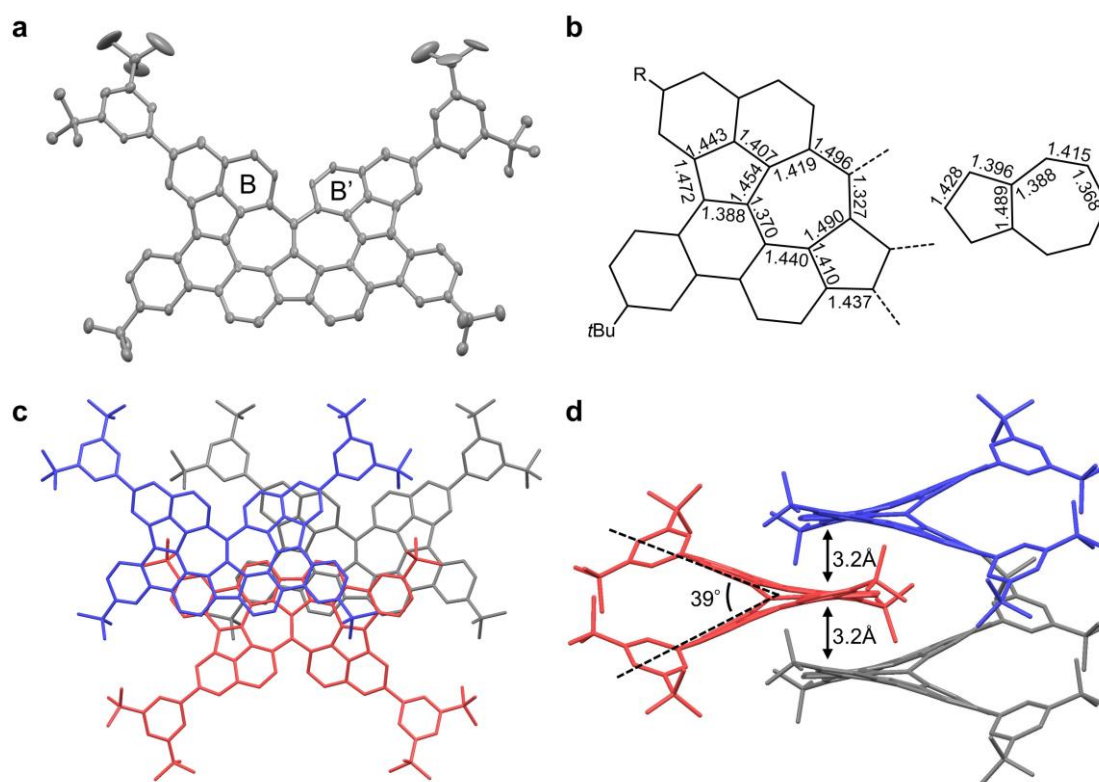

Fig. 3: Crystal structure of 1a. Hydrogen atoms and solvents are omitted for clarity. a, Top view (thermal ellipsoids are shown at 50% probability). **b**, Bond length of compound **1a** (left) and azulene (right). **c**, Top view and, **d**, side view of the packing structure in the crystal.

The strong intermolecular interactions of **1a** also led to an in-solution self-association behaviour: the ^{1}H NMR spectra of compound **1a** showed a significant concentration-dependence; that is, the peaks of aromatic protons shifted upfield as the concentration increased. These upfield-shifts resulted from face-to-face aggregations,[46] and the association constant (K_2) in CDCl$_3$/CS$_2$ (1:1) was estimated to be 74.1 ± 25.5 M^{-1} by assuming that dimers are formed predominantly[46,47] (see the Supporting Information for details). Interestingly, the degree of concentration dependence of the chemical shift varied significantly with the position of protons: the chemical shifts of the protons located on the planar region were considerably affected by the concentration, whereas those of the protons located around the cove region was not. These observations indicated that the in-solution self-aggregation was induced by the face-to-face π–π stacking interactions between the planar regions.

Since the cove-type structure of **1a** comprising of a contiguous 6–7–7–6 ring system was not investigated previously, we questioned if the racemisation barrier of this cove is high enough for **1a** to be chiral. Since the direct separation of compound **1a** by chiral HPLC was challenging due to its poor solubility, compound **1b**, whose aromatic substituent was replaced by a bulky tertiary alkyl side chain to increase its solubility, was prepared in a similar way. Compound **1b** exhibited a significantly improved solubility in common non-polar organic solvents (even in hexane), but not in polar solvents such as MeOH. Accordingly, **1b** was subjected to chiral HPLC analyses, and the

11

enantiomers were separated without any observable racemisation at 25 °C. The mirror-symmetric

circular dichroism (CD) spectra of the two separated fractions confirmed that they are certainly a

pair of enantiomers (Fig. 4a). The stable helicity of the cove of **1** is in clear contrast to that of the

normal cove structure comprising of four benzene rings, or [4]helicene structure, which is reported

to racemise immediately.[22,48] Theoretical calculations revealed that the free energy of activation for

the racemisation of the model structure (**1c**) is as high as 29.2 kcal/mol (Fig. 4b), which lies between

those of [5]helicene and [6]helicene (24.6 and 36.2 kcal/mol, respectively) (Fig. 4c).[49] The reason for

such a high racemisation barrier is that the hydrogen atoms of the cove region are forced to locate

closely to each other owing to the large interior angle of the 7-membered ring, requiring a highly

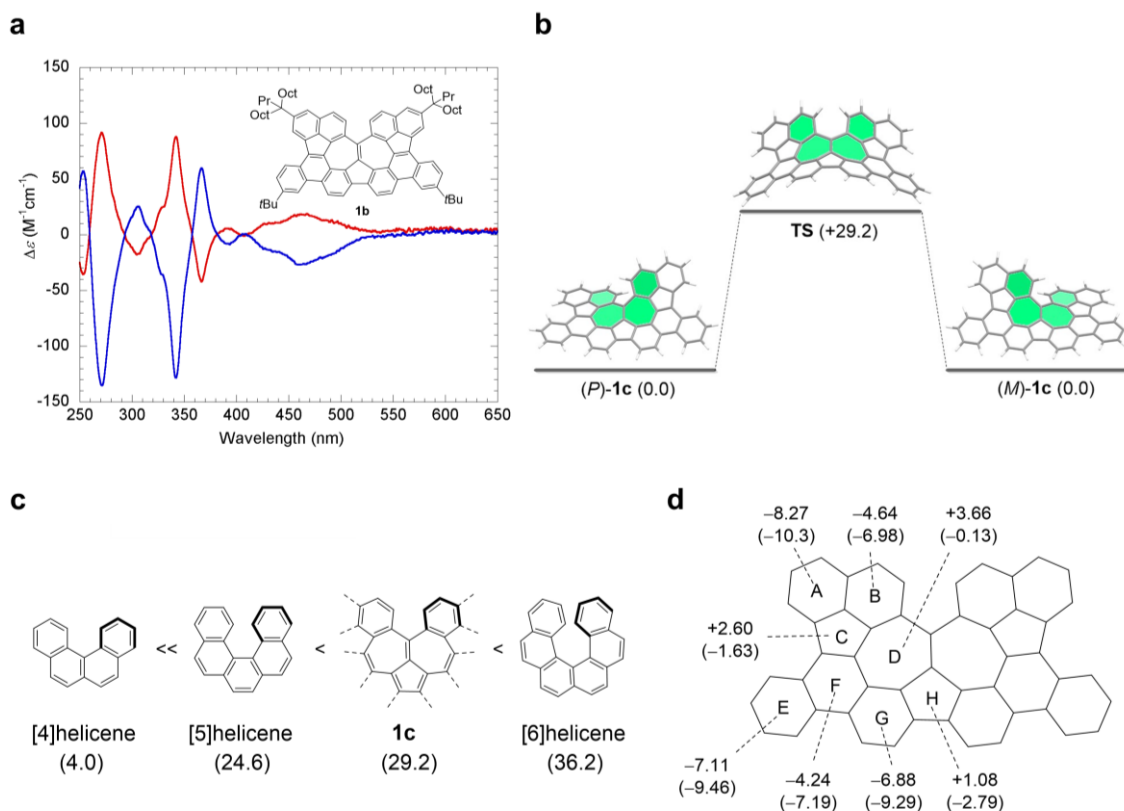distorted achiral transition state to undergo racemisation.

Fig. 4: Chirality and local aromaticity of AGN 1. a, CD spectra of **1b** (5.0×10^{-5} M in hexane). **b,**

Process for the racemisation of the model compound **1c**. Relative Gibbs free energies (kcal/mol) are

given in parentheses. Calculation was carried out at the B3LYP/6-31G(d,p) level of theory. **c,**

Comparison of the racemisation barriers among **1c** and helicenes. Free energies of activation

(kcal/mol) are shown in parentheses. **d**, NICS(0) and NICS(1) values of the model structure (**1c**).

Calculations were conducted at the GIAO-B3LYP/6-311+G(2d,p) level of theory. NICS(1) values

are given in parentheses. Structural optimisation was conducted at the B3LYP/6-31G(d) level of

theory.

The nucleus-independent chemical shifts (NICS) were calculated to gain insight into the local aromaticity of each ring in compound **1** (Fig. 4d). According to the calculations, all the hexagonal rings (A, B, E, F, and G) show negative NICS(1) values, confirming their aromatic characters. In more detail, the A–B ring system, which would be expected to have naphthalene-like property, shows larger NICS(1) values than that of naphthalene[50] (−10.7 ppm) especially for the B ring (−6.98 ppm), suggesting the weaker local aromaticity of these rings. Similarly, the phenanthrene-like E–F–G ring system shows larger NICS(1) values than that of unsubstituted phenanthrene.[50] The weaker local aromaticity of these hexagonal rings can be attributed to the π-conjugations between A–B and E–F–G ring systems through the embedded azulene structures. The pentagonal rings (C and H) and the heptagonal ring (D) show a slightly negative NICS(1) value, indicating that these rings have significantly weaker aromaticity than that of the unsubstituted azulene[50] (−7.82 and −17.8 ppm for heptagon and pentagon, respectively), presumably due to the fused benzene rings (A, B, F, and G).

To investigate the optoelectronic and electrochemical properties of **1**, UV-vis absorption spectroscopy, cyclic voltammetry (CV), and differential pulse voltammetry (DPV) were conducted. The UV-vis absorption spectra showed two weak bands at 660 and 600 nm, and strong bands at 477 and 404 nm in the visible region (Fig. 5a). According to the TD-DFT calculation, the weak bands at 660 and 600 nm could be assigned as HOMO $\rightarrow$ LUMO (λ_{calc} = 635 nm, f = 0.062) and HOMO–1 $\rightarrow$ LUMO transitions (λ_{calc} = 584, f = 0.036), respectively (Fig. 5b). We assigned the strong band at

480 nm to the contributions of HOMO $\rightarrow$ LUMO+1 ($\lambda_{calc} = 548$, $f = 0.247$) and HOMO‑2 $\rightarrow$

LUMO ($\lambda_{calc} = 513$, $f = 0.421$) transitions. According to the CV analysis, compound **1a** is stable to

both electrochemical oxidation and reduction; it shows three reversible oxidation peaks at 0.72, 0.83

and 1.2 V, and two reduction peaks at -1.3 and -1.7 V (vs. Ag/Ag$^+$) (Fig. 6a). In CV and DPV

voltammograms, the first oxidation peak was split into two small peaks (P1 and P2). Variable-

concentration DPV analysis of the soluble analogue **1b** suggested that this splitting of the oxidation

peaks resulted from the self-association characteristic of this compound (*vide supra*) (Fig. 6b). Since

the first peak (P1) weakened with a decrease in the concentration, it is considered to be due to the

oxidation of aggregated species. The second peak (P2), on the other hand, strengthened with a

decrease in the concentration, indicating that it results from the oxidation of monomeric species.
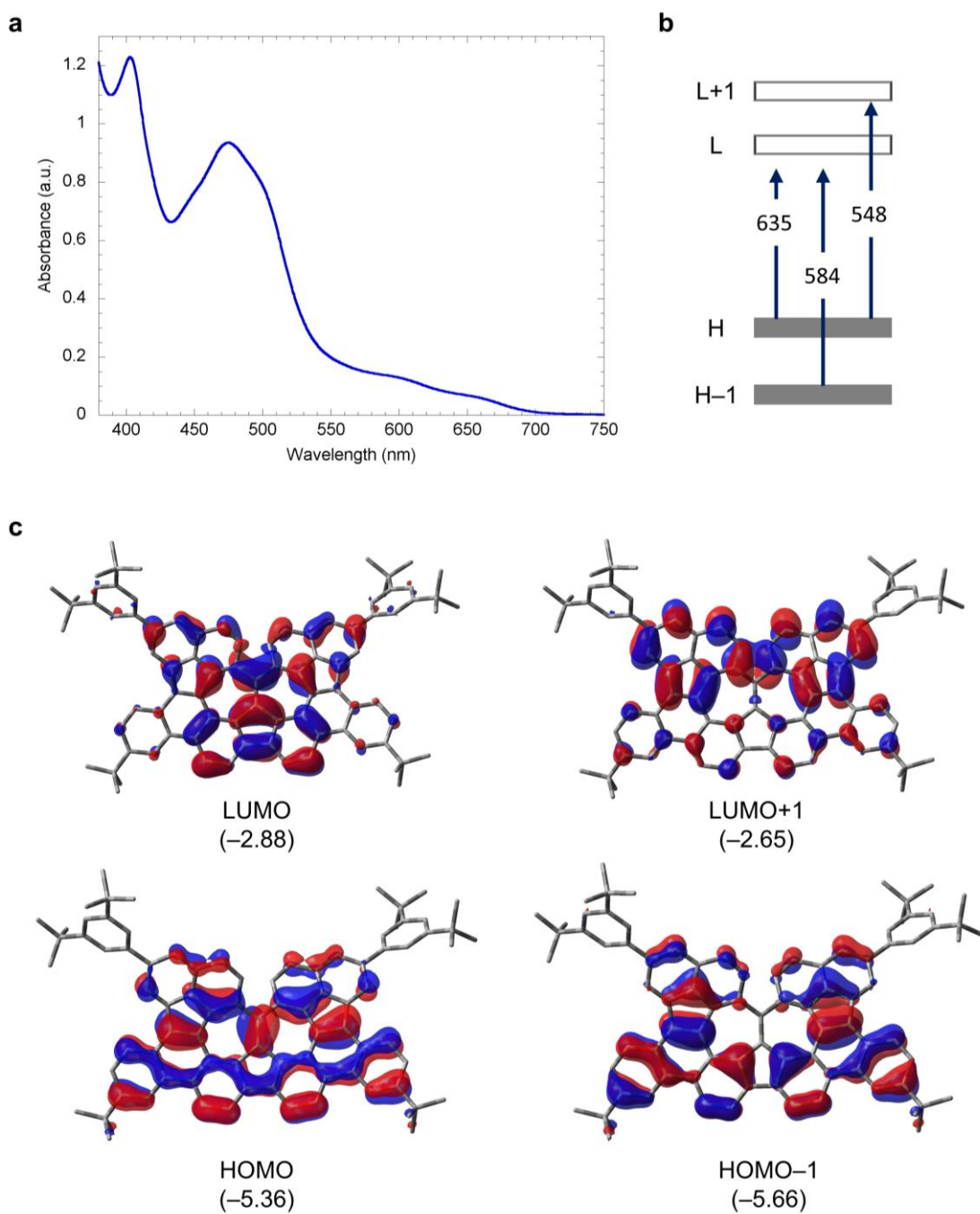
Fig. 5: Electronic properties of 1a. a, Experimental UV-vis absorption spectra of **1a** (1.0×10^{-4} M in

DCM). **b**, Major electronic transitions between frontier molecular orbitals of compound **1a**

calculated by the TD-DFT method at the B3LYP/6-311+G(d,p)-CPCM($CHCl_3$) level of theory.

Structural optimisation was conducted at the B3LYP/6-31G(d)-CPCM($CHCl_3$) level of theory. Wave

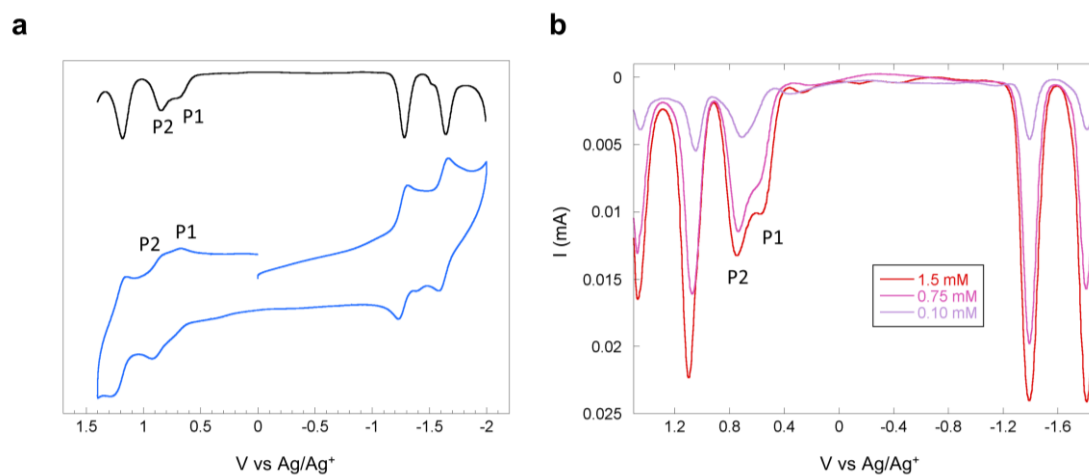lengths (nm) are given. **c**, Pictures of molecular orbitals of **1a**.

Fig. 6: Voltammograms of compounds 1a and 1b. a, Cyclic voltammogram (blue line) and differential pulse voltammogram (black line) of **1a** (1.0×10^{-4} M in DCM). **b**, Variable-concentration differential pulse voltammogram of **1b** (1.5×10^{-3}, 7.5×10^{-4}, and 1.9×10^{-4} M in DCM).

In summary, a new methodology for the construction of a highly condensed azulene unit was developed to synthesise graphene nanostructure **1** featured by the embedded azulene cluster and a narrowed variant of the cove edge. The cove-like region of **1** comprising a 6–7–7–6 ring system was demonstrated to have stable chirality both experimentally and theoretically, in contrast with those of structures with normal cove edges. Single crystal X-ray analysis, variable-concentration NMR, and DPV analyses revealed the tendency of **1** to stack via π–π interactions both in crystal form and in solutions. The new synthetic methodology and the information on the structural and electronic effect

of the azulene cluster in graphene nanostructure provided herein would contribute to the future

design and synthesis of various azulene-embedded nanocarbons.

Methods

Oxidative cyclisation of fluoranthene 2c. A solution of **2c** (16.2 mg, 40.0 μmol) and DDQ (20.0

mg, 88.0 μmol) in dry PrCN (4.0 mL) was irradiated with six 3.6 W blue LED strips for 60 h under

argon. The reaction mixture was then diluted with $CHCl_3$ and washed with saturated aqueous

$NaHCO_3$ followed by water. The organic phase was dried over $MgSO_4$, filtered through a pad of

silica gel, and then concentrated. The residue was purified by silica gel column chromatography

(hexanes/EtOAc) to recover compound **3c** (12.4 mg, 77% yield) as a purple solid.

Synthesis of 1a. To a stirred solution of **6** (603 mg, 0.541 mmol) and DDQ (270 mg, 1.19 mmol) in

dry DCM (60 mL), TfOH (0.47 mL, 5.4 mmol) was added. The mixture was stirred for 5 min and

quenched with Et_3N. The organic layer was washed with water, dried over $MgSO_4$, and concentrated.

Subsequently, the residue was dissolved in CS_2, filtered through a pad of silica gel, and concentrated.

After that, pentane was added to precipitate out the product, which was collected by filtration,

washed several times with MeOH followed by pentane, and dried under reduced pressure to recover

compound **1a** (95.2 mg, 16% yield) as a dark purple solid.

Data Availability

All data generated and analysed during this study are included in this Article and its Supplementary

Information. Crystallographic data for the structures reported in this Article have been deposited at

the Cambridge Crystallographic Data Centre, under deposition number CCDC 1995289 (**1a**). Copies

of the data can be obtained free of charge via www.ccdc.cam.ac.uk/data_request/cif.

References

1.   Yao, X. *et al.* Regioselective hydrogenation of a 60-carbon nanographene molecule toward a

        circumbiphenyl core. *J. Am. Chem. Soc.* **141**, 4230–4234 (2019).

2.   Chen, Q., Schollmeyer, D., Müllen, K. & Narita, A. Synthesis of circumpyrene by alkyne

        benzannulation of brominated dibenzo[*hi,st*]ovalene. *J. Am. Chem. Soc.* **141**, 19994–19999

        (2019).

3.   Zeng, W. *et al.* Superoctazethrene: An open-shell graphene-like molecule possessing large

        diradical character but still with reasonable stability. *J. Am. Chem. Soc.* **140**, 14054–14058

        (2018).

4.   Ajayakumar, M. R. *et al.* Toward full zigzag-edged nanographenes: Peri-tetracene and its

        corresponding circumanthracene. *J. Am. Chem. Soc.* **140**, 6240–6244 (2018).

5.   Gregolińska, H. *et al.* Fully conjugated [4]chrysaorene. Redox-coupled anion binding in a

tetraradicaloid macrocycle. *J. Am. Chem. Soc.* **140**, 14474–14480 (2018).

6.   Hitosugi, S. *et al.* Pentagon-embedded cycloarylenes with cylindrical shapes. *Angew. Chem. Int. Ed.* **56**, 9106–9110 (2017).

7.   Liu, J. *et al.* Unexpected Scholl reaction of 6,7,13,14-tetraarylbenzo[*k*]tetraphene: Selective formation of five-membered rings in polycyclic aromatic hydrocarbons. *J. Am. Chem. Soc.* **138**, 2602–2608 (2016).

8.   Cruz, C. M. *et al.* Enantiopure distorted ribbon-shaped nanographene combining two-photon absorption-based upconversion and circularly polarized luminescence. *Chem. Sci.* **9**, 3917–3924 (2018).

9.   Márquez, I. R. *et al.* Versatile synthesis and enlargement of functionalized distorted heptagon-containing nanographenes. *Chem. Sci.* **8**, 1068–1074 (2017).

10.   Kawasumi, K., Zhang, Q., Segawa, Y., Scott, L. T. & Itami, K. A grossly warped nanographene and the consequences of multiple odd-membered-ring defects. *Nat. Chem.* **5**, 739–744 (2013).

11.   Pun, S. H. *et al.* Synthesis, structures, and properties of heptabenzo[7]circulene and octabenzo[8]circulene. *J. Am. Chem. Soc.* **141**, 9680–9686 (2019).

12.   Michl, J. & Thulstrup, E. W. Why is azulene blue and anthracene white? a simple MO picture. *Tetrahedron* **32**, 205–209 (1976).

13.   Sun, Q. *et al.* On-surface synthesis of polyazulene with 2,6-connectivity. *Chem. Commun.* **55**,

13466–13469 (2019).

14.   Ma, J. *et al.* Helical Nanographenes containing an azulene Unit: Synthesis, crystal structures, and

        properties. *Angew. Chem. Int. Ed.* **59**, 5637–5642 (2020).

15.   Yamaguchi, Y. *et al.* Terazulene isomers: Polarity change of OFETs through molecular orbital

        distribution contrast. *J. Am. Chem. Soc.* **138**, 11335–11343 (2016).

16.   Xin, H. *et al.* Biazulene diimides: A new building block for organic electronic materials. *Chem.

        Sci.* **7**, 6701–6705 (2016).

17.   Nishimura, H. *et al.* Hole-transporting materials with a two-dimensionally expanded π-system

        around an azulene core for efficient perovskite solar cells. *J. Am. Chem. Soc.* **137**, 15656–15659

        (2015).

18.   Yazyev, O. V. & Louie, S. G. Topological defects in graphene: Dislocations and grain

        boundaries. *Phys. Rev. B* **81**, 195420 (2010).

19.   Vicarelli, L., Heerema, S. J., Dekker, C. & Zandbergen, H. W. Controlling defects in graphene for

        optimizing the electrical properties of graphene nanodevices. *ACS Nano* **9**, 3428–3435 (2015).

20.   Banhart, F., Kotakoski, J. & Krasheninnikov, A. V. Structural defects in graphene. *ACS Nano* **5**,

        26–41 (2011).

21.   Lu, J., Bao, Y., Su, C. L. & Loh, K. P. Properties of strained structures and topological defects in

        graphene. *ACS Nano* **7**, 8350–8357 (2013).

22. Liu, J. *et al.* Toward cove-edged low band gap graphene nanoribbons. *J. Am. Chem. Soc.* **137**, 6097–6103 (2015).

23. Nagarajan, K., Mallia, A. R., Muraleedharan, K. & Hariharan, M. Enhanced intersystem crossing in core-twisted aromatics. *Chem. Sci.* **8**, 1776–1782 (2017).

24. Sisto, T. J. *et al.* Long, Atomically precise donor-acceptor cove-edge nanoribbons as electron acceptors. *J. Am. Chem. Soc.* **139**, 5648–5651 (2017).

25. Yano, Y. *et al.* Step-growth annulative π-extension polymerization for synthesis of cove-type graphene nanoribbons. *J. Am. Chem. Soc.* **142**, 1686–1691 (2020).

26. Wu, J. *et al.* Cove-edged nanographenes with localized double bonds. *Angew. Chemie Int. Ed.* (2020). doi:10.1002/anie.202000326

27. Fan, Q. *et al.* Nanoribbons with nonalternant topology from fusion of polyazulene : Carbon allotropes beyond graphene. *J. Am. Chem. Soc.* **141***, 17713–17720 (2019).

28. Wang, Y. *et al.* Template effect in the competition between Haeckelite and graphene growth on Ni(111): Quantum chemical molecular dynamics simulations. *J. Am. Chem. Soc.* **133**, 18837–18842 (2011).

29. Narita, A., Wang, X. Y., Feng, X. & Müllen, K. New advances in nanographene chemistry. *Chem. Soc. Rev.* **44**, 6616–6643 (2015).

30. Segawa, Y., Ito, H. & Itami, K. Structurally uniform and atomically precise carbon

nanostructures. *Nat. Rev. Mater.* **1**, 15002 (2016).

31.   Yano, Y., Mitoma, N., Ito, H. & Itami, K. A quest for structurally uniform graphene nanoribbons:

        synthesis, properties, and applications. *J. Org. Chem.* **85**, 4–33 (2020).

32.   Ziegler, K. & Hafner, K. Eine rationelle Synthese des Azulens. *Angew. Chem.* **67**, 301–301

        (1955).

33.   Lellek, V. & Hansen, H. J. Surprising formation of highly substituted azulenes on thermolysis of

        4,5,6,7,8-pentamethyl-2h-eyelohepta[*b*]furan-2-one and heptalene formation with the new

        azulenes. *Helv. Chim. Acta* **84**, 1712–1736 (2001).

34.   Carret, S. *et al.* Approach to the blues: A highly flexible route to the azulenes. *Angew. Chem. Int.*

        Ed. **44**, 5130–5133 (2005).

35.   Hieulle, J. *et al.* On-surface route for producing planar nanographenes with azulene moieties.

        Nano Lett. **18**, 418–423 (2018).

36.   Liu, J. *et al.* Open-shell nonbenzenoid nanographenes containing two pairs of pentagonal and

        heptagonal rings. *J. Am. Chem. Soc.* **141**, 12011–12020 (2019).

37.   Mastalerz, M., Yang, X. & Rominger, F. Contorted polycyclic aromatic hydrocarbons with two

        embedded azulene units. *Angew. Chemie Int. Ed.* **58**, 17577–17582 (2019).

38.   Zhang, X. *et al.* Organic semiconductors dicyclohepta[*ijkl,uvwx*]rubicene with two pentagons and

        two heptagons as a stable and planar non-benzenoid nanographene. *Angew. Chem. Int. Ed.* **59**,

3529–3533 (2019).

39. Ogawa, N., Yamaoka, Y., Yamada, K. & Takasu, K. Synthesis of π-extended fluoranthenes via a KHMDS-promoted anionic-radical reaction cascade. *Org. Lett.* **19**, 3327–3330 (2017).

40. Mallory, F. B. & Mallory, C. W. Photocyclization of stilbenes and related molecules. *Org. React.* **30**, 1–449 (1984).

41. Villedieu-Percheron, E. *et al.* 6π/10π-Electrocyclization of ketene-iminium salts for the synthesis of substituted naphthylamines. *Tetrahedron Lett.* **55**, 2446–2449 (2014).

42. Gobbi, L. *et al.* Photoswitchable tetraethynylethene-dihydroazulene chromophores. *Helv. Chim. Acta* **84**, 743–777 (2001).

43. Miyaura, N. & Suzuki, A. Palladium-catalyzed cross-coupling reactions of organoboron compounds. *Chem. Rev.* **95**, 2457–2483 (1995).

44. Sheldrick, G. M. A short history of SHELX. *Acta Crystallogr. Sect. A Found. Crystallogr.* **64**, 112–122 (2008).

45. Dittrich, B. *et al.* Azulene revisited: solid-state structure, invariom modeling and lattice-energy minimization of a classical example of disorder. *Acta Cryst. B* **74**, 416–426 (2018).

46. Nakamura, K., Okubo, H. & Yamaguchi, M. Synthesis and self-aggregation of cyclic alkynes containing helicene. *Org. Lett.* **3**, 1097–1099 (2001).

47. Tobe, Y. *et al. m*-Diethynylbenzene macrocycles: Syntheses and self-association behavior in

solution. *J. Am. Chem. Soc.* **124**, 5350–5364 (2002).

48.   Barroso, J. *et al.* Revisiting the racemization mechanism of helicenes. *Chem. Commun.* **54**, 188–

191 (2017).

49.   Martin, R. H. & Marchant, M. J. Thermal racemisation of hepta-, octa-, and nonahelicene. Kinetic

results, reaction path and experimental proofs that the racemisation of hexa- and heptahelicene

does not involve an intramolecular double diels-alder reaction. *Tetrahedron* **30**, 347–349 (1974).

50.   Chen, Z., Wannere, C. S., Corminboeuf, C., Puchta, R. & von Ragué Schleyer, P. Nucleus-

independent chemical shifts (NICS) as an aromaticity criterion. *Chem. Rev.* **105**, 3842–3888

(2005).

Acknowledgements

Contributions

N.O. and K.T. developed the concept and conceived the experiments. N.O. performed the experiments. Y.Y., H.T., and K.Y. analysed the data. N.O. prepared the manuscript with assistance from K.T.

Ethics declarations

Competing interests

The authors declare no competing interests.

Supplementary information

Supplementary information and chemical compound information are available in the online version

of the paper. Reprints and permissions information is available online at www.nature.com/reprints.

Correspondence and requests for materials should be addressed to K.T.

Fig. 1: Azulene-embedded graphenes and graphene nanostructures. a, One example of a

graphene nanoribbon containing clusters of azulene units. **b,** Structures of "normal" cove edge. **c,**

"Narrowed" variant of cove edge. **d,** Structural design and synthetic strategy of nanographene **1**.

Fig. 2: Synthetic protocol for the azulene units. a, Conversion of dibenzofluoranthene **2** into

azulene 3 via visible-light-promoted oxidative cyclisation. **b,** Synthesis of AGN **1a.** Reaction

conditions: (a) Tf$_2$O, DIPEA, DCM, 25 °C (b) CH$_2$=C(Bpin)$_2$, K$_3$PO$_4$, Pd(PPh$_3$)$_4$, dioxane, 100 °C,

69% yield; (c) DDQ, butyronitrile, blue LEDs, 25 °C, 97% yield; (d) **5**, K$_3$PO$_4$, Pd(PPh$_3$)$_4$, dioxane,

100 °C, 46% yield; (e) DDQ, TfOH, DCM, 25 °C, 5 min, 16% yield. Tf = trifluoromethanesulfonyl;

DIPEA = diisopropylethylamine; DCM = dichloromethane; pin = pinacolate; DDQ = 2,3-dichloro-

5,6-dicyano-*p*-benzoquinone; LED = light emitting diode.

Fig. 3: Crystal structure of 1a. Hydrogen atoms and solvents are omitted for clarity. a, Top

view (thermal ellipsoids are shown at 50% probability). **b,** Bond length of compound **1a** (left) and

azulene (right). **c,** Top view and, **d,** side view of the packing structure in the crystal.

Fig. 4: Chirality and local aromaticity of AGN 1. a, CD spectra of **1b** (5.0×10^{-5} M in hexane). **b,**

Process for the racemisation of the model compound **1c**. Relative Gibbs free energies (kcal/mol) are given in parentheses. Calculation was carried out at the B3LYP/6-31G(d,p) level of theory. **c**, Comparison of the racemisation barriers among **1c** and helicenes. Free energies of activation (kcal/mol) are shown in parentheses. **d**, NICS(0) and NICS(1) values of the model structure (**1c**). Calculations were conducted at the GIAO-B3LYP/6-311+G(2d,p) level of theory. NICS(1) values are given in parentheses. Structural optimisation was conducted at the B3LYP/6-31G(d) level of theory.

Fig. 5: Electronic properties of 1a. a, Experimental UV-vis absorption spectra of **1a** $(1.0 \times 10^{-4}$ M in DCM). **b**, Major electronic transitions between frontier molecular orbitals of compound **1a** calculated by the TD-DFT method at the B3LYP/6-311+G(d,p)-CPCM(CHCl$_3$) level of theory. Structural optimisation was conducted at the B3LYP/6-31G(d) level of theory. **c**, Pictures of molecular orbitals of **1a**.

Fig. 6: Voltammograms of compounds 1a and 1b. a, Cyclic voltammogram (blue line) and differential pulse voltammogram (black line) of **1a** $(1.0 \times 10^{-4}$ M in DCM). **b**, Variable-concentration differential pulse voltammogram of **1b** $(1.5 \times 10^{-3}, 7.5 \times 10^{-4},$ and 1.9×10^{-4} M in DCM).